Title

Dynamics and Removal Pathway of Edge Dislocations in Imperfectly Attached PbTe Nanocrystal Pairs: Toward Design Rules for Oriented Attachment

Journal

ACS Nano, 12(4)

ISSN

1936-0851

Authors

Ondry, Justin C
Hauwiller, Matthew R
Alivisatos, A Paul

Publication Date

2018-04-24

DOI

10.1021/acsnano.8b00638

Peer reviewed

ACS NANO
Cite This: ACS Nano XXXX, XXX, XXX–XXX
www.acsnano.org

ARTICLE

Dynamics and Removal Pathway of Edge Dislocations in Imperfectly Attached PbTe Nanocrystal Pairs: Toward Design Rules for Oriented Attachment

Justin C. Ondry,[†,‡] Matthew R. Hauwiller,[†,‡] and A. Paul Alivisatos*[,†,‡,§,⊥]

[†]Department of Chemistry, University of California, Berkeley, California 94720, United States
[‡]Materials Sciences Division, Lawrence Berkeley National Laboratory, Berkeley, California 94720, United States
[§]Department of Materials Science and Engineering, University of California, Berkeley, California 94720, United States
[⊥]Kavli Energy NanoScience Institute, Berkeley, California 94720, United States

Supporting Information

ABSTRACT: **Using *in situ* high-resolution TEM, we study the structure and dynamics of well-defined edge dislocations in imperfectly attached PbTe nanocrystals. We identify that attachment of PbTe nanocrystals on both {100} and {110} facets gives rise to $b = a/2\langle 110\rangle$ edge dislocations. Based on the Burgers vector of individual dislocations, we can identify the glide plane of the dislocations. We observe that defects in particles attached on {100} facets have glide planes that quickly intersect the surface, and HRTEM movies show that the defects follow the glide plane to the surface. For {110} attached particles, the glide plane is collinear with the attachment direction, which does not provide an easy path for the dislocation to reach the surface. Indeed, HRTEM movies of dislocations for {110} attached particles show that defect removal is much slower. Further, we observe conversion from pure edge dislocations in imperfectly attached particles to dislocations with mixed edge and screw character, which has important implications for crystal growth. Finally, we observe that dislocations initially closer to the surface have a higher speed of removal, consistent with the strong dislocation free surface attractive force. Our results provide important design rules for defect-free attachment of preformed nanocrystals into epitaxial assemblies**

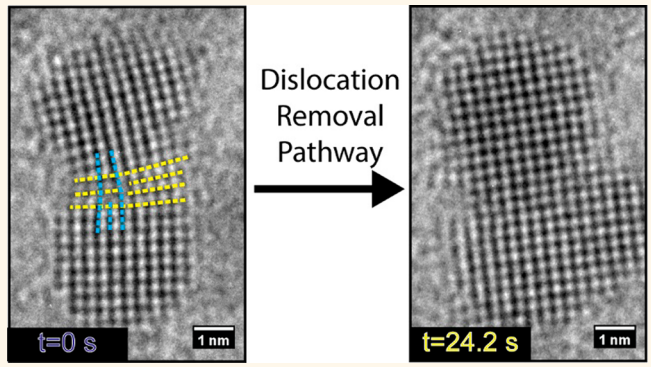

KEYWORDS: *nanocrystals, oriented attachment, dislocations, PbTe, self-assembly, in situ TEM*

Nanocrystals are sometimes considered perfect pieces of a single crystal because they are often free of nonequilibrium crystal defects such as dislocations and impurities. It is often thought that short diffusion lengths to surfaces where these defects can be removed facilitate the preparation of defect-free nanocrystals;[1−3] however, this is a topic of considerable debate.[4,5] There is little direct experimental evidence showing the mechanisms for defect removal in nanocrystals. Nonetheless, it would be desirable to leverage this lack of defects in individual particles as building blocks to make larger assemblies of epitaxially connected nanocrystals while maintaining low defect densities. The tunable atomic-like electronic states of individual semiconductor quantum dots behave like that of an artificial atom, and if strongly coupled by placing the quantum dots in an ordered array, the individual states could disperse into a band potentially leading to emergent properties that may not be exhibited by a natural material. Unfortunately, as synthesized, the nanocrystals have long organic ligands on the surface that prevent the necessary coupling. However, there has been progress getting around this by creating epitaxially connected arrays of nanocrystals through oriented attachment with a variety of structures.[6−11] These structures are theorized to have exotic electronic properties, but they have not been realized experimentally.[12−15] Defects that arise from the attachment process may be preventing the realization of these exotic electronic structures.[16,17] Without a microscopic understanding

Received: January 24, 2018
Accepted: February 22, 2018
Published: February 22, 2018

DOI: 10.1021/acsnano.8b00638
ACS Nano XXXX, XXX, XXX–XXX

of defect removal mechanisms and the size dependence of these mechanisms in nanocrystals, it will be difficult to realize the goal of creating perfect epitaxial connected assemblies of nanocrystals.

Oriented attachment is the proposed mechanism though which nanoparticles are epitaxially joined.[18−24] In this process, particles first spontaneously organize so that they share a common crystallographic orientation; then the particles fuse to create a crystallographically coherent interface. The shape of the nanocrystals, faceting, and the ligand coverage all can mediate the attachment process.[25] It is believed that this process plays an important role in some mineralization processes[26] and the growth of certain types of anisotropic nanostructures.[22,23,27] Oriented attachment of a pair of nanocrystals provides a starting point for understanding the basic unit of nonclassical aggregative crystal growth[28,29] that is active in oriented attachment growth of materials with zero-, one-, two-, and three-dimensional structures (dots,[30,31] rods,[22,23,27] sheets,[32−34] and bulk solids,[26] respectively). In the ideal case, oriented attachment produces perfect interfaces. However, it is well known that when nanocrystals undergo oriented attachment, if a step edge exists on the surface of one of the particles, it can create an edge dislocation in the attached structure,[18,35] and attachment of multiple particles can give rise to screw dislocations.[36] These dislocations have several implications for classical crystal growth and semiconductor properties. Screw dislocations, for example, provide self-propagating step edges on the surface, allowing crystals to grow by monomer attachments at much lower supersaturations than expected for perfect surfaces.[37−40] In addition, dislocations in semiconductors are scattering centers for charge carriers, and they can introduce midgap trap states, which can cause carriers to localize and recombine.[41,42] By understanding the necessary conditions (time, temperature, nanocrystal size, *etc.*) required for removal of dislocations from a single imperfect oriented attachment event, we can begin to design syntheses such that a defect that arises from an imperfect oriented attachment event is removed before subsequent attachment events occur, thus preventing the accretion and trapping of defects deep in the material. Further, there is likely a strong size dependence for defect mobility, and by understanding this we can determine upper limits for size of attaching particles, where defect removal is still achieved in a reasonable amount of time.

The close proximity of any given point in a nanocrystal to the surface further complicates understanding the size scaling of defect motion since it is known there is a strong dislocation surface interaction.[43] From a continuum elasticity standpoint, this can be understood through the image force construction of dislocation−free-surface interactions in semi-infinite crystals. Forces on a dislocation at a free surface is modeled as that between the dislocation in the material and a mirror dislocation of opposite sign placed in the vacuum opposite the interface.[43] In this model, the force pulling a dislocation to the surface depends strongly on the distance that dislocation is from the surface and is given, for an edge dislocation, by eq 1.

$$\frac{F}{L} = \frac{\mu b^2}{4\pi(1-\nu)l} \tag{1}$$

where $\frac{F}{L}$ is the force per unit length on the dislocation, μ is the shear modulus, ν is the Poisson ratio, b is the magnitude of the burgers vector, and l is the distance between the dislocation and free surface. Based on eq 1, dislocation surface interactions should play a large role in driving dislocations out of nanocrystals faster than expected from a purely diffusion-based argument. In nanocrystals, this is somewhat more complicated because there are several surfaces near the dislocation, and thus several superimposed forces act on a dislocation. Finite element methods have been used to more accurately account for this and other complications such as surface and shape relaxations expected in nanocrystals.[44] Even with these considerations, the highly nonlinear distance-dependent force on dislocations only cancels out for the exact center of a symmetrically shaped nanocrystal (*e.g.*, cube, sphere) and is an unstable mechanical equilibrium.[45] The barrier to removal of a dislocation in this case is now limited by the Peierls barrier, which is the activation barrier the dislocation must surmount in order to glide.[46] If the image forces experienced by a dislocation are larger than the Peierls stress of the dislocation, which is the shear stress necessary to overcome the Peierls barrier, it will be driven to the surface, resulting in a dislocation-free nanocrystal.[47,48] While the importance of dislocation surface interactions in nanocrystals and nanograins has been explored theoretically, only *ex post facto* transmission electron microscopy (TEM) images of structurally perfect nanocrystals and nanograins below a critical size provide indirect experimental evidence in support of these ideas.[49]

Understanding size-dependent defect stability is important for the preparation of epitaxially connected superlattices of nanocrystals through oriented attachment since it puts an upper limit on the size of particles that can likely be attached while maintaining perfect fidelity. There are many pathways to defects in these materials; for example, it has been shown that the inherent size distribution of the nanocrystals used for attachment leads to places where nanocrystals in the epitaxial superlattices are not connected[16] and that improving the connectivity is necessary for realizing delocalized carriers.[50] Another potential defect that may be limiting the performance of these materials are dislocations introduced during the stochastic attachment process (see for example the SI of ref 53). Understanding how these defects can be removed from attached nanocrystals will likely be necessary to create high-quality materials. There are examples of *in situ* TEM observations where defects from imperfect oriented attachment are removed from the attached particles either thermally[51] or with electron beam stimulation.[52] However, in these examples, the experiments were not performed with the particles perfectly aligned on a zone axis, which prevented identification of important parameters describing the dislocations such as the Burgers vector. Without the knowledge of the Burgers vector, the behavior of a dislocation in a nanocrystal cannot be compared to dislocation theory[43] to determine if these well-established ideas apply to nanomaterials.

Dislocation theory provides geometric rules that govern how a defect can move in a material and may give insight for designing defect-free attachment of nanocrystals. Most examples of epitaxial superlattices use materials that have the rock salt crystal structure (PbS, PbSe, and PbTe). In the following, we introduce dislocation theory considerations for attaching rock salt nanocrystals. It is commonly understood that oriented attachment typically occurs on nonpolar facets of crystals; thus for the rock salt crystal structure both the {100} and {110} facets can be used for attachment. Indeed, epitaxial superlattices have been made by attaching PbX (X = S, Se) particles on either the {100} and {110} facets, suggesting that both routes are viable for preparing these epitaxial super-

DOI: 10.1021/acsnano.8b00638
ACS Nano XXXX, XXX, XXX−XXX

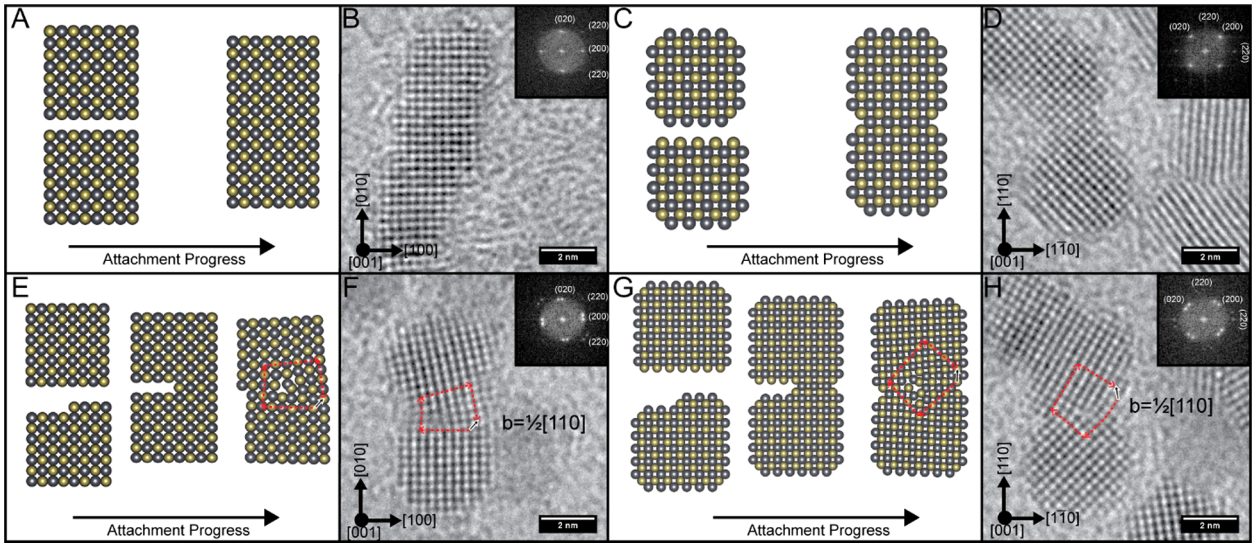

Figure 1. (A) Schematic representation of the process leading to perfect attachment of PbTe nanocrystals on {100} facets and (B) experimental HRTEM image and corresponding FFT of three PbTe nanocrystals that have attached perfectly on the {100} facets. (C) Schematic representation of the process leading to perfect attachment of PbTe nanocrystals on {110} facets and (D) experimental HRTEM image and corresponding FFT of two PbTe nanocrystals that have attached perfectly on the {110} facets. (E) Schematic representation of a step edge leading to a $b = a/2[110]$ edge dislocation during the attachment of PbTe nanocrystals on {100} facets. Red dotted arrows outline the Burgers circuit with the Burgers vector shown with a white outlined black arrow. (F) Experimental HRTEM image and corresponding FFT of PbTe nanocrystals attached imperfectly on {100} facets with a $b = a/2[110]$ Burgers vector. (G) Schematic representation of a step edge leading to a $b = a/2[110]$ edge dislocation during the attachment of PbTe nanocrystals on {110} facets. (H) Experimental HRTEM image and corresponding FFT of PbTe nanocrystals attached imperfectly on {110} facets with a $b = a/2[110]$ Burgers vector.

lattices.[53] However, this does not consider the potential for crystalline defect formation and removal. In the rock salt crystal system, the lowest energy edge dislocation that can be formed has a Burgers vector $b = a/2\langle 110\rangle$. The glide plane, which is the plane that it is easiest for a dislocation to move in, is defined by the plane normal given by $b \times \xi$ where ξ is the sense vector collinear with the dislocation line.[43] For a dislocation to be glissile (able to move), the glide plane of the dislocation must coincide with one of the slip planes of the crystal system hosting the dislocation.[43] In the case of PbS, PbSe, and PbTe, in bulk the observed slip planes are {100}; however this is likely from two sets of $\langle 110\rangle$ dislocations whose shear sums to $\langle 002\rangle$,[43] and TEM studies on PbS indicate both {100} and {110} slip planes are active for $b = a/2\langle 110\rangle$ dislocations.[54] Thus, {110} planes are possible slip panes in these crystals and $b = a/2\langle 110\rangle$ dislocations are glissile. If a $b = a/2\langle 110\rangle$ edge dislocation was formed at the interface between two PbX particles attaching on {100} facets, no matter the exact relationship between the attachment direction and Burgers vector, the glide plane will always intersect the surface of the particles even in the case of attaching multiple particles into a lattice (see SI Figure S1 for visualization of all possible Burgers vector and glide plane permutations for {100} and {110} attachment). Instead, if they are attached on {110} facets, for certain configurations of the Burgers vector and attachment direction, the glide plane is collinear with attachment direction, meaning the dislocation has a large distance to travel before reaching the surface. In this case, attaching multiple particles into a lattice would require the dislocation traverse a quasi-infinite distance in the glide plane before it is annihilated at the surface. These simple geometric arguments suggest that, for the rock salt crystal system, it should be far easier to remove edge dislocations when the particles are attached on {100} facets compared to those attached on the {110} facets.

In this work, we show using high-resolution transmission electron microscopy (HRTEM) that PbTe nanocrystals attached on either {100} or {110} facets produce $b = a/2\langle 110\rangle$ edge dislocations. Further, we show using *in situ* HRTEM that with electron beam stimulation the $b = a/2\langle 110\rangle$ edge dislocation in {100} attached particles quickly glides to the surface easily, producing a defect-free interface between the particles, whereas, the $b = a/2\langle 110\rangle$ edge dislocation in a {110} attached particle undergoes a complex trajectory involving dislocation glide, climb, and conversion to a screw dislocation all while not reaching the surface even after an order of magnitude longer time exposed to the same electron dose rate. Further we analyze the misorientation angle between the two imperfectly attached crystallites and find it is consistent with the continuum elastic solution to an edge dislocation in a thin plate. In addition, we provide evidence that the speed of dislocation removal depends on the initial distance of that dislocation from the surface, which is qualitatively consistent with the image force description of dislocations at free surfaces. Finally, we discuss how our results indicate two points that should be considered when epitaxially attaching nanocrystals: (1) Once anisotropy has been introduced into a nanostructure, the relationship of the glide plane of possible dislocations and the attachment direction becomes an important consideration for removing dislocations from nanomaterials. (2) Smaller attachment interfaces are more easily made defect free because of strong image forces pulling potential defects out of the material.

RESULTS

Epitaxial attachment between individual PbX nanocrystals can be induced through several methods such as heating nanocrystal superlattices on a liquid subphase,[53] chemically treating them to remove surface ligands,[7,50] or simply diluting the

DOI: 10.1021/acsnano.8b00638
ACS Nano XXXX, XXX, XXX−XXX

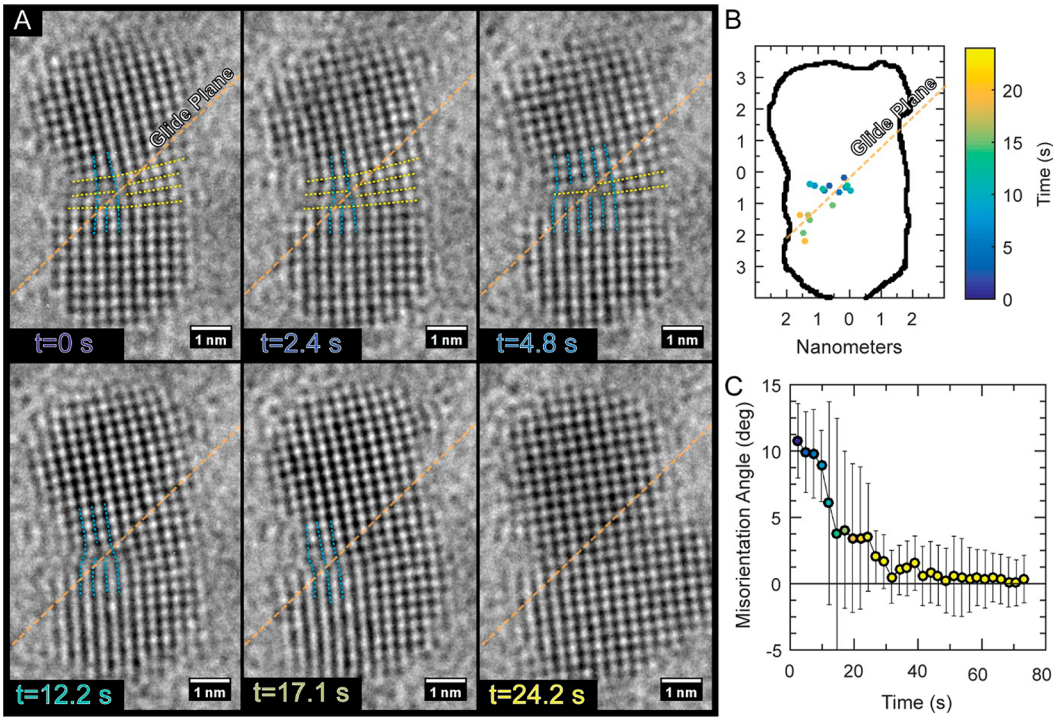

Figure 2. (A) Evolution of the b = 1/2[110] edge dislocation position during ~4000 $e^-/Å^2$·s electron beam irradiation of the two PbTe nanocrystals attached imperfectly on {100} facets. Selected HRTEM images with dark atom contrast from the time series showing the dislocation removal process. Blue and yellow lines are overlaid on the (100) and (010) planes, respectively, as guides to the eye. The color of each time stamp corresponds to the colorbar in (B). (B) The dislocation position was determined from geometric phase analysis of a time series of HRTEM images. The color of each dot corresponds to the time. Overlaid is the glide plane of the dislocation determined from the Burgers vector. (C) Misorientation angle of the two crystallites as a function of time. The color of each point corresponds to the colorbar in (B). Error bars represent the standard deviation of the rotation value difference across the two crystallites determined by geometric phase analysis.

particles sufficiently to desorb bound surface ligands. We found that dilution of the nanocrystal surface ligands during solvent processing with toluene or *ortho*-dichlorobenzene to sandwich ~4.0 nm oleate capped PbTe nanocrystals (synthesis, TEM, and size distribution shown in Figure S2) between sheets of graphene was sufficient to induce significant attachment of particles on both {100} and {110} facets (Figure 1A–D and Figure S3). We found that it was important to maintain rigorous oxygen- and moisture-free conditions during purification and handling of the PbTe nanocrystals to observe epitaxial nanocrystal attachment. Synthesis was performed on a Schlenk line with ultrapure argon (<5 ppm of O_2), which was further purified to <1 ppb O_2 by a Nupure III prepurifier. Nanocrystals were cleaned in an argon glovebox (<1 ppm of O_2 and H_2O) using anhydrous acetone and dissolved in anhydrous toluene. TEM samples were prepared in a N_2-filled glovebox (<1 ppm of O_2 and H_2O) and quickly (~3 min air exposure) transferred to the TEM column. Lead chalcogenide nanocrystal surfaces are easily oxidized likely to PbX/PbO or PbX/$PbXO_3$ (X = Se, Te) surfaces,[55,56] which even a small amount would be sufficient to prevent epitaxial attachment. Due to the low temperature and somewhat uncontrolled nature of the oriented attachment with this sample preparation strategy, we could observe nanocrystals that had undergone both perfect and imperfect oriented attachment. In addition, the nearly cubic shapes of the starting nanocrystals lead to preferential orientation of the particles on ⟨100⟩ zone axes, which is ideal for HRTEM observation due to the large lattice spacing in that direction and the ability to observe $b = a/2\langle 110\rangle$ edge dislocations.

Figure 1 overviews different attachment processes that can give rise to perfect and imperfect attachment on either {100} or {110} facets. A schematic representation of the attachment process of PbTe nanocrystals that do not contain step edges on {100} facets is shown in Figure 1A. We experimentally observed the perfect attachment of PbTe nanocrystals on {100} facets (Figure 1B) by HRTEM imaging with dark atom contrast. The inset fast Fourier transform (FFT) shows sharp spots consistent with a single-crystalline domain and no crystal misorientation. Figure 1C shows a process that can lead to perfect attachment of PbTe nanocrystals on {110} facets. We note in the model when viewed as a projection down the ⟨001⟩ zone axis, it appears that a Te-rich facet is reacting with a Pb-rich facet, but {110} facets are indeed nonpolar and consist of alternating layers of the two elements. We experimentally observed the perfect attachment of PbTe nanocrystals on {110} facets (Figure 1D), and the inset FFT shows a single-crystal pattern consistent with no misorientation. In these experiments, attachment of particles on {100} facets was observed much more frequently than {110} facets (Figure S3). We suspect that the higher ratio of {100} faceting of our nanocrystals, observed by HRTEM of the particles before attachment (Figure S2C), could lead to a greater probability of this attachment pathway; however other effects such as ligand binding strength to the different facets may have an effect.

Most of the time, perfect attachment between particles was observed. In surveying our samples across 33 μm^2 and 258

DOI: 10.1021/acsnano.8b00638
ACS Nano XXXX, XXX, XXX–XXX

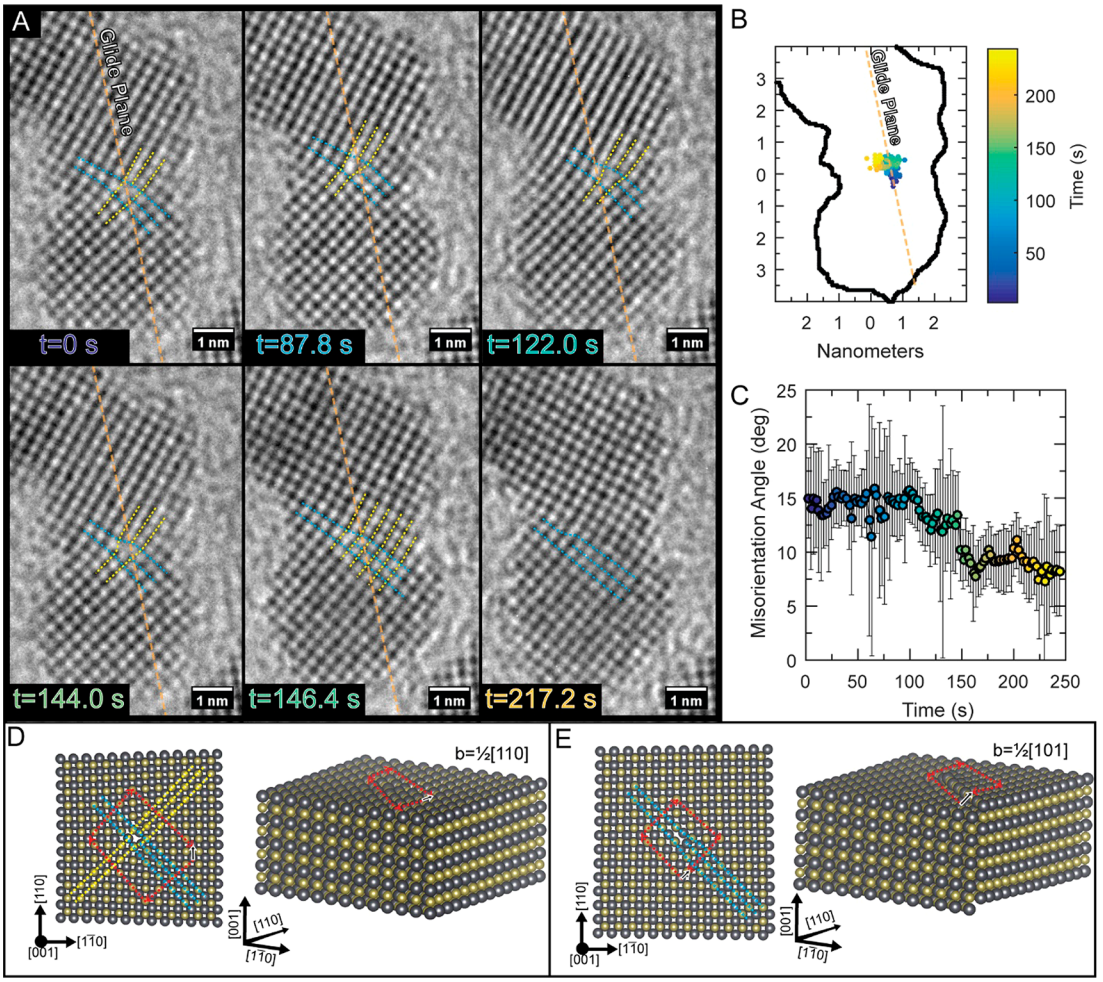

Figure 3. (A) Evolution of the $b = a/2[110]$ edge dislocation position during ~4000 $e^-/Å^2$·s electron beam irradiation of the two PbTe nanocrystals attached imperfectly on {110} facets. Selected HRTEM images with dark atom contrast from the time series showing the dislocation removal process. Blue and yellow lines are overlaid on the (100) and (010) planes, respectively, as guides to the eye. The color of each time stamp corresponds to the colorbar in (B). (B) The dislocation position was determined from geometric phase analysis of a time series of HRTEM images. The color of each dot corresponds to the time. Overlaid is the glide plane of the dislocation determined from the Burgers vector. (C) Misorientation angle of the two crystallites as a function of time. The color of each point corresponds to the colorbar in (A). Error bars represent the standard deviation of the rotation value difference across the two crystallites determined by geometric phase analysis. Particularly large standard deviations for certain points come from suboptimal images where the GPA indicated a greater variation the rotation maps. (C) Plan view (left) and tilted (right) models of dislocations in PbTe with pure edge $b = a/2[110]$ character (D) and mixed edge and screw $b = a/2[101]$ character (E).

attachment events, ~80% of the particles had perfect interfaces. The rest were attached with a mixture of high angle tilt boundaries and imperfect oriented attachment. Imperfect oriented attachment that generated edge dislocations was observed for particles attached on both {100} and {110} facets. Figure 1E shows schematically how a step edge on a {100} facet can yield a $b = a/2\langle 110\rangle$ edge dislocation. Red dotted arrows outline a Burgers circuit around a dislocation with a white outlined black arrow for the Burgers vector following the right-hand start finish convention with a dislocation sense going into the page. We experimentally observed similar edge dislocations with Burgers vectors of $b = a/2\langle 110\rangle$ at the interface between two PbTe nanocrystals (Figure 1F). The formation of this dislocation is unsurprising since this is the lowest energy dislocation for the rock salt crystal structure.[43] In addition, the step edge necessary for the particles to imperfectly attach and yield a $b = a/2\langle 110\rangle$ edge dislocation is relatively common in the particles used for attachment (Figure S2C). The inset FFT shows two distinct spots for the {100} spacing coming from the two distinct nanocrystal domains that are misoriented by the dislocation.

We also observed that dislocations form at the interface where particles attach on {110} facets. Figure 1G shows a schematic process for the generation of a $b = a/2\langle 110\rangle$ edge dislocation due to a step edge on a {110} facet of one of the particles. We experimentally observed a $b = a/2\langle 110\rangle$ edge dislocation at the interface of two particles that attached on {110} facets. The inset FFT shows two distinct spots that correspond to the two misoriented nanoparticle domains. It is interesting that dislocations with the same Burgers vector are formed from attachment of different facets, although this is unsurprising since the $b = a/2\langle 110\rangle$ edge dislocation is the lowest energy, and there are reasonable surface faceting that can give rise to the same dislocation for both facets. The data suggest that the energetics of the dislocation formation dictates the type of dislocation formed, rather than the facet that is attaching for this material. We observed the formation of $b = a/2\langle 110\rangle$ edge dislocations on both {100} and {110} attached

DOI: 10.1021/acsnano.8b00638
ACS Nano XXXX, XXX, XXX−XXX

particles on multiple occasions (Figure S4), indicating this type of defect formation is common. Another common defect in the rock salt crystal structure is a dislocation with a Burgers vector $b = a\langle 100\rangle$. We did not observe any instance of this dislocation. This dislocation has a higher elastic energy, which goes as b^2, and thus we suspect this makes it less favorable to form. Further the formation of a $b = a\langle 100\rangle$ edge dislocation would require a two atomic layer {100} step edge, which we observe few of in the original PbTe nanoparticle sample (Figure S2C).

Next, we wanted to understand if $b = a/2\langle 110\rangle$ edge dislocations are more easily removed from particles attached on {100} facets compared to {110} facets, which is what would be predicted based on the simple geometric arguments in the introduction. To this end, we collected HRTEM movies of the imperfectly attached particles under ∼4000 $e^-/Å^2{\cdot}s$ electron beam irradiation. Recent experimental and theoretical studies have indicated that electron beam irradiation can induce sample excitations similar to thermal excitation;[57−59] thus performing our experiments at the same dose rate should allow us to compare dislocation dynamics in different samples. Under these conditions we could collect movies with sufficient resolution to track the dislocation as it evolved (Movie S1). Figure 2A shows selected frames from the TEM movie of {100} imperfectly attached particles showing the dislocation moves in its glide plane to the surface of the particle, where it is annihilated within 24 s. The overlaid blue and yellow lines correspond to the (100) and (010) planes, which show the extra (100) and (010) plane that is expected for a $b = a/2\langle 110\rangle$ edge dislocation. At $t = 12.2$ s and $t = 17.1$ s, we could not distinguish the (010) planes definitively; we suspect the bottom crystal is rotating so quickly during the collection of these frames (1 s) that the atom columns are getting blurred. To objectively track the dislocation position as a function of time, we performed geometric phase analysis (GPA) on each frame of the movie to measure the experimental strain field in the attached particles. Then, the position of the discontinuity in the strain field was taken to be the position of the dislocation for that fame (details in Figure S5). The position of the dislocation is plotted in Figure 2B, where the color of each dot corresponds to the time. The edge of the nanocrystal is outlined in black. Overlaid on the plot is the glide plane for the dislocation determined from the Burgers vector, clearly showing the dislocation following the {110} glide plane directly to the surface of the particle. In addition, we determined the average misorientation angle between the two particles by taking the difference of the average value of the rotation image from geometric phase analysis for each of the two particles (Figure S6). The error bars were determined by measuring the standard deviation of the rotation value, determined by GPA, for each crystallite and adding the standard deviations in quadrature. These error bars are a metric both for the intrinsic error in the measurement and for variations in the orientation across individual crystallites due to strains imposed by the dislocation or quick rotation of the lattice during image acquisition. The misorientation angle as a function of time is plotted in Figure 2C, where the color of each point corresponds to the colorbar in Figure 2B to facilitate comparison. We observe that the misorientation angle between the particles decreases as the dislocation approaches the surface. Further, in frames where one of the crystallites is rapidly changing and shows spatial variation of orientation, such as the bottom crystallite at the $t = 12.2$ s time point, a larger standard deviation in the misorientation angle is measured.

To test our hypothesis that $b = a/2\langle 110\rangle$ edge dislocations would be more difficult to remove from {110} attached particles, we performed the same experiment as above (with the same electron dose rate) on {110} imperfectly attached particles (Movie S2). Snapshots from this movie are shown in Figure 3A. Initially, the dislocation moves in the glide plane ($t = 0-87$ s), but this movement does not bring it any closer to the surface of the particle. This is further highlighted in the dislocation position map determined by geometric phase analysis (Figure 3B). In addition to glide, we briefly observe the dislocation move closer to the particle surface ($t \approx 122$ s) seen both in the dislocation position map and in the HRTEM image (Figure 3A, $t = 122.0$ s). While this appears to be progressing toward removing the dislocation from the material, it is happening on a much slower time scale than we observed for {100} attachment. The slower rate is consistent with dislocation climb,[43] where a dislocation moves out of its glide plane to an adjacent one. However, in dislocation climb, vacancies must coalesce with the dislocation to move it out of the current glide plane, meaning the speed of this process depends on the vacancy concentration in the material and is typically much slower than dislocation glide. Further we observe a small, ∼3°, decrease in the misorientation angle (Figure 3C) after the dislocation undergoes dislocation climb, moving it closer to the surface ($t = 122$ s), and the source of the angle change will be discussed later. After the dislocation climb event, the dislocation undergoes a complex trajectory, which will be discussed later, but importantly even after 217 s of 4000 $e^-/Å^2{\cdot}s$ the particle still contains a defective interface (Figure 3A). This is consistent with our hypothesis that the collinear glide plane and attachment direction would lead to more difficult dislocation removal.

In addition to dislocation climb, we observe other types of dislocation dynamics later in this defect's trajectory. In two subsequent frames (Figure 3A, $t = 144.0$ to 146.4 s), we first observe the defect with orthogonal (100) and (010) extra half-planes, consistent with a $b = a/2\langle 110\rangle$ edge dislocation. In the subsequent frame, only the extra (100) plane is present. Based on this projection it would appear that the system now has a $b = a/2\langle 100\rangle$ edge dislocation, yet that Burgers vector is not allowed in the rock salt crystal system and does not make physical sense because it would result in Pb−Pb and Te−Te bonds (Figure S7). However, if we consider out-of-plane, $a/2[001]$, character to the Burgers vector of the new dislocation, a sensible structure can be deduced. In this case, the dislocation now has partial screw character. Figure 3D and E show a crystal model of a dislocation with pure edge ($b = a/2[110]$) character and with partial screw character ($b = a/2[101]$), respectively. It is clear based on the structural model in Figure 3E that when viewed along the [001] zone axis, only the (100) extra half-plane would be observed. We performed multislice HRTEM image simulations of a $b = a/2[101]$ mixed dislocation, and the simulated image is consistent with the experimental image (Figure S8). We note that we cannot determine the handedness of the screw dislocation based on TEM, and the equivalent $b = a/2[10\bar{1}]$ is also possible. The tilted models and overlaid Burgers circuit on the right of each panel highlight the out-of-plane character of the proposed screw dislocation. In addition, we observe a ∼5° decrease in in-plane misorientation angle when the dislocation converts to partial screw character, consistent with a decrease in edge character of the dislocation, which is what gives rise to the in-plane misorientation. Furthermore, we would expect a tilt around the attachment

DOI: 10.1021/acsnano.8b00638
ACS Nano XXXX, XXX, XXX−XXX

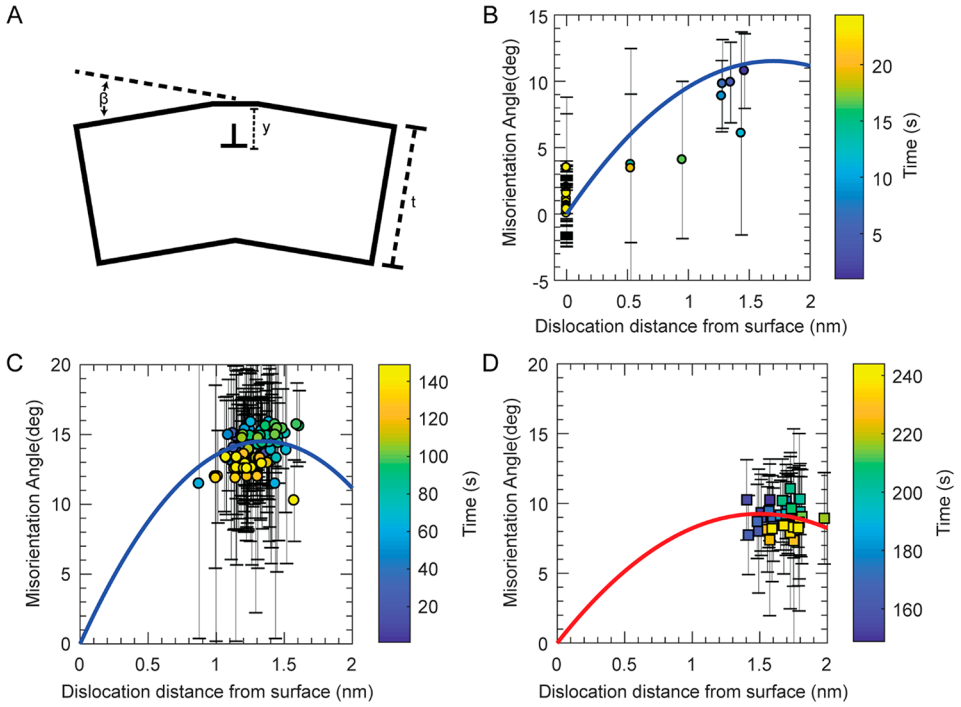

Figure 4. (A) Schematic representation of a dislocation in a thin plate described in eq 1. (B) Misorientation angle as a function of dislocation distance from the surface for the $b = a/2[110]$ edge dislocation in the {100} attached particles shown in Figure 2. (C) Misorientation angle as a function of dislocation distance from the surface for the $b = a/2[110]$ edge dislocation in the {110} attached particles shown in Figure 3. In both cases, the line is a plot of eq 1 using the measured thickness of the crystal at the defect and a $b = a/2[110]$ Burgers vector. (D) Misorientation angle as a function of dislocation distance from the surface for the mixed dislocation from Figure 3 observed after conversion to partial screw character. The line is a plot of eq 1 for the $b = a/2[100]$ edge component of the dislocation. We note that upon conversion to screw character, the dislocation moved toward the *opposite* surface of the particle, and eq 1 is defined across the whole thickness of the particle and is simply a maximum at the exact middle.

[110] axis of the crystallites if a screw dislocation was present. This can be thought of as a small slice of a twist boundary between two grains, which has a characteristic twist angle given by $\theta = b_{screw}/D$ where D is the spacing between screw dislocations.[60] In this case, the spacing of screw dislocations can be approximated at the neck thickness, and thus we would expect a twist of approximately 5° between the two crystallites. This twist could be manifested as a decrease in contrast due to one of the particles rotating off the ⟨001⟩ zone axis. Indeed, we observed several cases of screw dislocations (Figure S10) where one of the particles appears to be rotated off zone axis while the other remains on the ⟨001⟩ zone axis. To corroborate this, we performed multislice TEM image simulations of tilted 3.8 nm PbTe cuboctahedra-shaped nanocrystals (Figure S11), which showed that a 5° rotation off the ⟨001⟩ zone axis was sufficient to result in reduced contrast in the planes whose surface normal is perpendicular to the rotation axis. This evidence further supports the conversion from edge to mixed dislocations in imperfectly attached nanocrystals. Finally, we observe edge to mixed conversion multiple times (Figure S9), indicating that this process is common in imperfectly attached PbTe nanocrystals where the defect takes a significant amount of time to anneal out.

Based on our data, there is a strong interplay between the misorientation of the two crystallites, the dislocation distance from the surface, and the dislocation character. The misorientation angle between the crystallites on both {100} and {110} attachment is much larger than expected for an isolated dislocation in an infinite crystal. However, we realized the geometry of these attached particles is the same as an edge dislocation in a thin plate.[61,62] The isotropic continuum elasticity solution for this dislocation geometry has been solved, and it predicts that the misorientation angle of the crystal on either side of the crystal depends on the magnitude of the Burgers vector, dislocation distance from surface, and crystal thickness according to eq 2 (adopted and rearranged from refs 61 and 62).

$$\beta = \frac{6by(t - y)}{t^3} \tag{2}$$

where β is the misorientation angle in radians, b is the magnitude of the Burgers vector in Å, y is the dislocation distance from the surface in Å, and t is the crystal thickness in Å. Figure 4A shows the geometry and variables described in this equation. This equation provided reasonable predictions for 160 nm thick SnS_2 foils with edge dislocations by careful angle measurements using convergent beam electron diffraction,[61] and recently modern synchrotron based μ-Laue diffraction experiments of misorientation in GaAs thin foil with a single dislocation showed that a continuum model accurately predicted misorientation angles.[63] Using the dislocation position and misorientation angle that we have determined from the geometric phase analysis, we plotted the misorientation angle as a function of dislocation distance from the surface for the {100} attached particles in Figure 4B. We observe that the misorientation angle decreases as the dislocation approaches the surface. Further, we measured the crystal thickness at the dislocation position and plotted eq 2 for that thickness. We can see particularly when the dislocation is far from the surface, eq 2 provides a good prediction for the

DOI: 10.1021/acsnano.8b00638
ACS Nano XXXX, XXX, XXX−XXX

misorientation angle. We performed the same analysis for the {110} attached particles. In this case, we separated the analysis into the regime before conversion to a mixed dislocation (Figure 4C) and after conversion to a mixed dislocation (Figure 4D). In the mixed case, only the magnitude of the edge component ($b_{edge} = a/2[100]$) is input in eq 2 for the Burgers vector since the screw component does not contribute to the in-plane misorientation. In both cases, the agreement between eq 2 and the experimental data is quite good. Unfortunately for the {110} trajectory, the dislocations did not approach the surface; thus the validity of the equation could not be evaluated as the dislocation approached the surface. Furthermore, the {100} attached particles (Figures 2 and 4B) had a larger contact area between the two crystals and thus a smaller misorientation angle than the {110} attached crystals (Figures 3 and 4C), which is consistent with the inverse relationship between misorientation angle and thickness in eq 2. Taken together, misorientation angles observed in imperfectly attached particles are consistent with the predictions from a simple continuum elasticity model.

Thus far, we have carefully analyzed the trajectories of two dislocations; however we wanted to determine if our hypothesis that dislocation removal is easier for {100} attached particles was significant across multiple particles. To do this, we evaluated the dynamics for several particles attached on both facets to determine the average removal speed for those dislocations and understand the generality of our observation. We defined the average removal speed by first measuring the shortest distance between the initial position of the dislocation and the surface; then we determined how long it took the particle to achieve a perfect interface. The dislocation removal speeds at the same electron dose rate for five different particles (Movies S1–S5) are shown in Figure 5. We observe that for

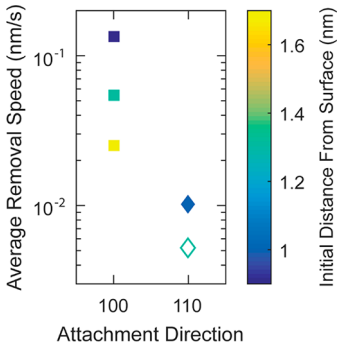

Figure 5. Average dislocation removal speed for particles attached on the {100} (squares) and {110} (diamonds) facets. The speed was determined by measuring the shortest distance between dislocation and the surface and dividing it by the total time needed to achieve a perfect particle. The color of each point shows the initial distance of the dislocation from the surface. All data points were taken at an electron dose rate of ~4000 $e^-/Å^2$·s. Solid points correspond to particles that achieved perfect interfaces within the observation time; open points did not.

particles attached on {100} facets the dislocation is removed more quickly than for those attached on {110} facets. In addition, we observe that the initial distance the dislocation is from the surface has a strong effect on the average removal speed. This indicates that the closer a dislocation is to the surface, the faster it moves toward the surface. This is qualitatively consistent with the attractive force expected between a dislocation and a surface based on the image force representation of dislocation surface interactions.[43] Indeed, across several attachment events, {100} attachment provides much easier dislocation removal compared to {110} attachment in the rock salt crystal system.

DISCUSSION

On the Importance of Attachment Direction and Size for Dislocation Removal from Nanocrystals. We observe that $b = a/2\langle 110\rangle$ edge dislocations that result from {100} attachment are much easier to remove than {110} attachment for the rock salt crystal structure. This is consistent with our hypothesis that the collinear glide plane and attachment direction would lead to more difficult dislocation removal. Our results indicate that care must be taken when attaching nanoparticles to ensure that the glide plane of the dislocation formed intersects a surface. More generally, once anisotropy is induced in a nanoparticle, defects cannot be ignored since it is possible for a dislocation to have a glide plane that does not intersect the surface of the particle. Further, since different materials have different slip systems and low-energy dislocations, the attachment directions that are ideal will depend on the crystal structure of the material. In addition, our results imply that many of these undesirable dislocations can be avoided if the starting nanocrystals were free of step edges on the surface. Currently, there is a lack of methods to characterize this parameter in ensembles of nanocrystals, and thus it is unclear which synthetic parameters must be tuned to make smooth nanocrystal surfaces. Careful consideration of these dislocation removal design rules will be important for preparing defect-free epitaxial nanoparticle assemblies.

The image force representation of the dislocation surface interactions provides an additional consideration for attachment. A dislocation near the surface is far easier to remove because the distance the dislocation must diffuse to reach the surface is less and because the force pulling the dislocation to the surface increases as the dislocation approaches the surface. The first takeaway is that oriented attachment of small particles is much more likely to produce defect-free interfaces because potential interfacial defects are much easier to heal. In support of this, there are several examples in the literature of the preparation of single-crystal extended nanostructures that appear to be free of dislocations though the attachment of small (<3 nm) particles.[64−68] Further, these considerations indicate that when attaching larger particles, controlling the shapes such that smaller epitaxial necks form may be better because the small necks will be much easier to heal if imperfectly attached. In the context of epitaxial superlattice assembly, this result indicates that the shape of the starting particles should be controlled such that small necks form initially, and then the necks can be thickened using postsynthetic reactions.[69] In the specific case for lead chalcogenide nanocrystals, the ideal shape for epitaxial attachment would be truncated cuboctahedra where the small {100} terminating facets are induced to attach, and any defects which may form are easily removed. However, as the desired attachment facet is made smaller, it may increase the likelihood of attachment happening on different facets. Thus, a balance will need to be found between smaller attachment facets needed to minimize defects and larger facets to ensure facet selective epitaxial connections. The limited diffusion length and surface image force, where the importance of the latter has not been fully appreciated until now, combine to greatly facilitate

DOI: 10.1021/acsnano.8b00638
ACS Nano XXXX, XXX, XXX−XXX

defect removal from colloidal nanomaterials. This explains the ease of preparation of defect-free colloidal nanocrystals of many materials at modest temperatures compared to their bulk melting temperatures. These ideas can be extended to provide guidelines for attaching nanocrystals while maintaining their perfect crystal lattices.

Conversion to Mixed Dislocations and Its Implications for Classical Crystal Growth and Nanocrystal Synthesis. Understanding how a pure edge dislocation converts to a screw dislocation is important because the latter are difficult to remove and serve as spots for monomer attachment. From a continuum elasticity standpoint, a screw dislocation has a lower strain energy than a pure edge dislocation with the same magnitude of Burgers vector; thus it is not unexpected that the dislocation converts to partial screw character.[43] The time scale of the conversion is intriguing because it happens within 1 frame in our HRTEM movie (1.4 s readout time between frames). In addition, there is essentially a discontinuity in the misorientation angle between the two particles when the conversion occurs, which further highlights the speed of the conversion. One possible mechanism for this conversion is the collective shearing in the ⟨011⟩ direction in the (010) slip plane. Considering the finite number of atomic planes that this occurs over, this mechanism is only reasonable and possible in the smallest nanocrystals. On the other hand, a kink in the dislocation with screw character could also nucleate and propagate rapidly to convert the dislocation to partial screw character. With this mechanism, screw conversion could occur regardless of nanocrystal size since the kink nucleation activation barrier is not as strongly size dependent. Future studies on the size-dependent dislocation dynamics in nanocrystals with better time resolution should be able to answer this question.

It was previously hypothesized that imperfect orientated attachment between two particles would likely only give rise to edge dislocations because there is a significant driving force for crystals to achieve full coherence around an axis normal to the attachment direction. Thus, imperfect oriented attachment of two particles would not give rise to screw dislocations.[36] The only confirmed mechanism for generating screw dislocations in nanocrystals is imperfect oriented attachment of three or more particles where one particle lays across a low-angle tilt boundary between the two other particles.[36] Our results show that it is possible for a pure edge dislocation in *two* attached particles to convert to a dislocation with partial screw character. This shows there are alternative ways to form screw dislocations during imperfect particle attachment. We observed conversion to mixed dislocations in many instances of *two* attached particles with either {100} or {110} attachment (Figure S9), and some already had mixed character initially (Figure S10). It is unclear if they contained mixed character initially, or if they converted during the electron beam exposure while searching and focusing. Importantly, once a screw dislocation is formed, it provides a self-propagating step edge for monomer attachment based crystal growth.[37,40] Screw dislocations are often cited as the source of step edges that allows for crystal growth to occur at far lower supersaturations than expected if the surface of crystals were perfect. Our results show an additional pathway for the formation of those defects, which could have important implications for further understanding of crystal growth and mineralization processes.

Further, from the standpoint of removing dislocations from imperfectly attached nanocrystals, the character of the dislocation has important consequences. Typically screw dislocations are less mobile than edge dislocations because of larger Peierls barriers,[43,70] and this is the case for rock salt crystals.[71,72] Thus, once the screw dislocation forms, it will be even harder to remove. In addition, the image force experienced by a screw dislocation at a free surface is smaller than an edge dislocation with the same magnitude of Burgers vector,[43] meaning the critical size for defect free nanocrystals is smaller for screw dislocation free materials.[47] The combination of larger Peierls barriers and smaller image forces make screw dislocations the most difficult to remove from a nanocrystal. This is observed experimentally in Figure 3A, where over the course of almost 100 s the mixed dislocation remains in essentially the same location in the crystal. This further highlights the importance of removing the dislocations from nanocrystals quickly to minimize the likelihood of making dislocations with screw character, which are harder to remove.

Understanding the Misorientation between Imperfectly Attached Nanocrystals. It is interesting to consider the mechanisms giving rise to the misorientation angle between the two crystallites. The ability of individual nanocrystal domains to freely misorient without needing to strain the surrounding crystal causes them to misorient more than expected compared to a dislocation cut from a bulk crystal. Further, we observe that the misorientation angle between the crystallites decreases as the dislocation approaches the surface. We can understand this by considering the same dislocation geometry as Figure 4A. If the dislocation moves upward, the interface below the dislocation increases in length, and it becomes less favorable for a large misorientation angle to be present because a larger number of bonds are highly strained if the angle remains large. Likewise, as the misorientation angle decreases, fewer atomic bonds are highly strained above of the dislocation and thus are not as great of an energy penalty for the misorientation angle to decrease. This behavior is quantitively captured in a continuum elasticity model by eq 2. It is surprising that an isotropic continuum model can predict the misorientation angles measured in the nanocrystals considering the size and discreteness of the bonding at these length scales. We can understand this by considering how the discrete lattice will affect the energy of the system. The continuum model neglects the dislocation core energy, which corresponds to the nonelastic energy at the center where the atom displacements are large. Typically, the dislocation core energy is much smaller than the elastic contributions. Further, changes in misorientation angle may only have a small effect on the magnitude of the core energy. Thus, we suspect the core energy change with misorientation angle will have a small effect on the overall energy of the system compared to the elastic energy reduction that results from misorienting the crystals. Further understanding of the details of the misorientation angle in imperfectly attached nanocrystals will require more detailed size-dependent studies and comparison with results from continuum elastic theories, molecular dynamics simulations, and *ab initio* calculations.

CONCLUSION

We have studied the dynamics of $b = a/2\langle 110\rangle$ edge dislocations in PbTe nanocrystals that have imperfectly attached on {100} and {110} facets. For particles attached on the {100} facets, the dislocation follows its glide plane, which lies 45° to the surface, and quickly yields a perfect interface. For particles attached on the {110} facets, the glide plane is

DOI: 10.1021/acsnano.8b00638
ACS Nano XXXX, XXX, XXX−XXX

collinear with the attachment direction. In this case, the dislocation moves in its glide plane initially, but this does not bring the particle any closer to the surface. Instead, the dislocation undergoes a complex trajectory including dislocation climb and conversion to a screw dislocation. These trends were realized across multiple particles by measuring the dislocation removal speed, which showed that particles attached on {100} facets became perfect an order of magnitude more quickly than for those attached on {110} facets. We believe that our results reveal several important considerations regarding crystalline defects in nanocrystals. First, once anisotropy is introduced in a structure, the relationship between the glide plane of the dislocation and the anisotropy direction becomes important. In addition, the observation of pure edge dislocations converting to screw dislocations provides a source of self-propagating step edges, which are important growth sites for monomer attachment driven crystal growth. Relating to epitaxially connected superlattices of nanocrystals, our results suggest that attachment of PbX particles on the {100} facets will make it easier to remove defects than those attached on {110} facets. Further we provide direct experimental evidence for dislocation surface attractive interactions in nanocrystals, which highlights the highly nonlinear scaling of defect removal kinetics in nanocrystals. To put this in context, II–VI and IV–VI nanocrystals have been successfully prepared with high material quality. However, the development of colloidal nanocrystals of more covalent materials (III–V and IV materials), which have higher Peierls barriers and thus smaller defect-free critical sizes, with high material quality lags. Higher temperatures, which are limited in colloidal synthesis, are thus needed to anneal out defects in a reasonable amount of time. With a fundamental understanding of size-dependent defect stability and dynamics in nanocrystals, it may be possible to design colloidal syntheses that may prevent defect formation or facilitate removal, thus realizing high-quality III–V and IV materials colloidally. The behavior of defects in nanocrystals and how well-developed dislocation theory can describe extended defects in small (<5 nm) volumes is a relatively underexplored field, and further understanding will be needed to continue the drive to synthesize nanomaterials with ever-increasing material quality.

MATERIALS AND METHODS

Materials. PbO lead(II) oxide 99.9% Sigma; oleic acid 90% (OA) technical grade Aldrich; octadecene 90% (ODE) technical grade Aldrich; *n*-trioctylphosphine 97% (TOP) Strem; tellurium shot 99.9999% Alfa Aesar; CVD graphene on copper 3–5 layer ACS materials; Quantifoil R1.2/1.3 300 mesh Au holey carbon SPI supplies. All solvents used were purchased as anhydrous with Sure Seal lids and sparged with argon prior to bringing into an argon-filled glovebox.

Nanocrystal Synthesis. PbTe nanocrystals were synthesized based on modified methods from Zhu *et al.*[73] A 1.0 M TOP–Te solution was prepared by dissolving tellurium shot in TOP in an argon glovebox (<1 ppm of O_2 and H_2O) at room temperature for ~36 h. Next, 900 mg of PbO, 7.56 g of OA, and 16 g of ODE were loaded in a three-neck round-bottom flask and heated under vacuum on a Schlenk line at 100 °C for 1 h to complex lead oleate and dry the solution. The flask was refilled with argon (ultrapure <1 ppm of O_2) 3× and heated to 120 °C. A 2 mL amount of the 1.0 M TOP–Te solution was injected, and the nanocrystals were allowed to grow for 10 min at 120 °C. The reaction was quenched by quickly cooling to room temperature using a water bath. The nanocrystals were cannula transferred to a Schlenk flask and transferred to an argon glovebox. The nanocrystals were washed 3× by precipitating them with excess acetone, centrifuging, and dissolving the resulting pellet in toluene. The sample were stored in an argon glovebox. It was found that pristine unoxidized surfaces were necessary for ligand displacement mediated attachment.

TEM Sample Preparation. Graphene-coated TEM grids were prepared by direct transfer of 3–5 layer graphene onto holey quatifoil TEM grids.[74] PbTe particles sandwiched between graphene sheets where prepared based on modified methods for making graphene veils and sandwiches.[75] Briefly, in a glovebox a small droplet of dilute PbTe nanocrystals in toluene was dropped on a graphene-coated TEM grid, and the droplet was allowed to dry. A second graphene-coated TEM grid was placed on top, and a droplet of toluene or orthodichlobenzene was placed on the sandwich. This assembly was covered with a glass dish, and the solvent was allowed to slowly evaporate for several hours to seal the sample between the graphene. The sample was taken out of the glovebox and quickly (~3 min) transferred to the TEM column.

TEM Imaging. TEM imaging was performed on a FEI Tecnai T20 S-TWIN TEM operating at 200 kV with a LaB_6 filament. Images were taken near Scherzer focus, which resulted in dark atom contrast for this crystal thickness. Time series of TEM images were collected with a Gatan Orius SC200 using a custom digital micrograph script with full 2048 × 2048 pixel readout, at a nominal magnification of 400k×, resulting in a pixel resolution of 0.13 Å/pixel, an exposure time of 1s, and a readout time of 1.4 s, yielding a frame rate of 0.4 fps. Since the defect dynamics were beam initiated, care was taken to minimize electron dose prior to imaging. Searching was performed with a spread beam; then once a suitable defective nanoparticle was found, a custom Digital Micrograph script was used to condense the beam to reproducibly return to the same dose rate within a session for each movie acquisition. We estimate a dose rate of ~4000 $e^-/Å^2 \cdot s$ was used for all data collected.

ASSOCIATED CONTENT

Supporting Information

The Supporting Information is available free of charge on the ACS Publications website at DOI: 10.1021/acsnano.8b00638.

Video S1: HRTEM movie of {100} imperfectly attached PbTe nanocrystals shown in Figure 2; Video S2: HRTEM movie of {110} imperfectly attached PbTe nanocrystals shown in Figure 3; Video S3: HRTEM movie and bandpass-filtered HRTEM movie of {100} imperfectly attached PbTe nanocrystals used to get removal time for Figure 5; Video S4: HRTEM movie and bandpass-filtered HRTEM movie of {110} imperfectly attached PbTe nanocrystals used to get removal time for Figure 5; Video S5: HRTEM movie of {100} imperfectly attached PbTe nanocrystals used to get removal time for Figure 5(ZIP)

Figures S1–S11 (PDF)

AUTHOR INFORMATION

Corresponding Author

*E-mail: paul.alivisatos@berkeley.edu.

ORCID

Justin C. Ondry: 0000-0001-9113-3420

Matthew R. Hauwiller: 0000-0002-5448-6937

A. Paul Alivisatos: 0000-0001-6895-9048

Notes

The authors declare no competing financial interest.

Additional Data: The raw TEM data presented here as well as the different steps in the data analysis for Figures 2 and 3 are available on the DASH repository at https://doi.org/10.6078/D17675.

DOI: 10.1021/acsnano.8b00638
ACS Nano XXXX, XXX, XXX–XXX

ACKNOWLEDGMENTS

The work was supported by the U.S. Department of Energy, Office of Science, Office of Basic Energy Sciences, Materials Sciences and Engineering Division, under Contract No. DE-AC02-05-CH11231, within the Physical Chemistry of Inorganic Nanostructures Program (KC3103). The authors would like to thank Prof. Jillian F. Banfield, Prof. Wendy Gu, and Prof. Matthew R. Jones for useful discussions.

REFERENCES

(1) Dalpian, G.; Chelikowsky, J. Self-Purification in Semiconductor Nanocrystals. *Phys. Rev. Lett.* **2006**, *96*, 226802.
(2) Turnbull, D. Formation of Crystal Nuclei in Liquid Metals. *J. Appl. Phys.* **1950**, *21*, 1022−1028.
(3) Alivisatos, P. Nanoscience — Potential and Threats. *Mol. Front. J.* **2017**, *1*, 50−65.
(4) Du, M. H.; Erwin, S. C.; Efros, A. L.; Norris, D. J. Comment On "self-Purification in Semiconductor Nanocrystals. *Phys. Rev. Lett.* **2008**, *100*, 179702.
(5) Dalpian, G. M.; Chelikowsky, J. R. Dalpian and Chelikowsky Reply. *Phys. Rev. Lett.* **2008**, *100*, 179703.
(6) Boneschanscher, M. P.; Evers, W. H.; Geuchies, J. J.; Altlantzis, T.; Goris, B.; Rabouw, F. T.; van Rossum, S. A. P.; van der Zant, H. S. J.; Siebbeles, L. D. A.; Van Tendeloo, G.; Swart, I.; Hilhorst, J.; Petukhov, A. V.; Bals, S.; Vanmaekelbergh, D. Long-Range Orientation and Atomic Attachment of Nanocrystals in 2D Honeycomb Superlattices. *Science* **2014**, *344*, 1377−1380.
(7) Walravens, W.; De Roo, J.; Drijvers, E.; Ten Brinck, S.; Solano, E.; Dendooven, J.; Detavernier, C.; Infante, I.; Hens, Z. Chemically Triggered Formation of Two-Dimensional Epitaxial Quantum Dot Superlattices. *ACS Nano* **2016**, *10*, 6861−6870.
(8) Baumgardner, W. J.; Whitham, K.; Hanrath, T. Confined-but-Connected Quantum Solids *via* Controlled Ligand Displacement. *Nano Lett.* **2013**, *13*, 3225−3231.
(9) Whitham, K.; Hanrath, T. Formation of Epitaxially Connected Quantum Dot Solids: Nucleation and Coherent Phase Transition. *J. Phys. Chem. Lett.* **2017**, *8*, 2623−2628.
(10) Sandeep, C. S. S.; Azpiroz, J. M.; Evers, W. H.; Boehme, S. C.; Moreels, I.; Kinge, S.; Siebbeles, L. D. A.; Infante, I.; Houtepen, A. J. Epitaxially Connected PbSe Quantum-Dot Films: Controlled Neck Formation and Optoelectronic Properties. *ACS Nano* **2014**, *8*, 11499−11511.
(11) Singh, A.; Singh, A.; Ong, G. K.; Jones, M. R.; Nordlund, D.; Bustillo, K.; Ciston, J.; Alivisatos, A. P.; Milliron, D. J. Dopant Mediated Assembly of Cu2ZnSnS4Nanorods into Atomically Coupled 2D Sheets in Solution. *Nano Lett.* **2017**, *17*, 3421−3428.
(12) Kalesaki, E.; Evers, W. H.; Allan, G.; Vanmaekelbergh, D.; Delerue, C. Electronic Structure of Atomically Coherent Square Semiconductor Superlattices with Dimensionality below Two. *Phys. Rev. B: Condens. Matter Mater. Phys.* **2013**, *88*, 1−9.
(13) Beugeling, W.; Kalesaki, E.; Delerue, C.; Niquet, Y.-M.; Vanmaekelbergh, D.; Morais Smith, C. Topological States in Multi-Orbital HgTe Honeycomb Lattices. *Nat. Commun.* **2015**, *6*, 6316.
(14) Kalesaki, E.; Delerue, C.; Morais Smith, C.; Beugeling, W.; Allan, G.; Vanmaekelbergh, D. Dirac Cones, Topological Edge States, and Nontrivial Flat Bands in Two-Dimensional Semiconductors with a Honeycomb Nanogeometry. *Phys. Rev. X* **2014**, *4*, 1−12.
(15) Butler, M. R.; Movaghar, B.; Marks, T. J.; Ratner, M. A. Electron Pairing in Designer Materials: A Novel Strategy for a Negative Effective Hubbard U. *Nano Lett.* **2015**, *15*, 1597−1602.
(16) Savitzky, B. H.; Hovden, R.; Whitham, K.; Yang, J.; Wise, F.; Hanrath, T.; Kourkoutis, L. F. Propagation of Structural Disorder in Epitaxially Connected Quantum Dot Solids from Atomic to Micron Scale. *Nano Lett.* **2016**, *16*, 5714−5718.
(17) Reich, K. V.; Shklovskii, B. I. Exciton Transfer in Array of Epitaxially Connected Nanocrystals. *ACS Nano* **2016**, *10*, 10267−10274.
(18) Li, D.; Nielsen, M. H.; Lee, J. R. I.; Frandsen, C.; Banfield, J. F.; De Yoreo, J. J. Direction-Specific Interactions Control Crystal Growth by Oriented Attachment. *Science* **2012**, *336*, 1014−1018.
(19) Sarkar, S.; Acharya, S.; Chakraborty, A.; Pradhan, N. Zinc Blende 0D Quantum Dots to Wurtzite 1D Quantum Wires: The Oriented Attachment and Phase Change in ZnSe Nanostructures. *J. Phys. Chem. Lett.* **2013**, *4*, 3292−3297.
(20) Yong, K. T.; Sahoo, Y.; Zeng, H.; Swihart, M. T.; Minter, J. R.; Prasad, P. N. Formation of ZnTe Nanowires by Oriented Attachment. *Chem. Mater.* **2007**, *19*, 4108−4110.
(21) Zhang, H.; De Yoreo, J. J.; Banfield, J. F. A Unified Description of Attachment-Based Crystal Growth. *ACS Nano* **2014**, *8*, 6526−6530.
(22) Koh, W.; Bartnik, A. C.; Wise, F. W.; Murray, C. B. Synthesis of Monodisperse PbSe Nanorods: A Case for Oriented Attachment. *J. Am. Chem. Soc.* **2010**, *132*, 3909−3913.
(23) Cho, K.-S.; Talapin, D. V.; Gaschler, W.; Murray, C. B. Designing PbSe Nanowires and Nanorings through Oriented Attachment of Nanoparticles. *J. Am. Chem. Soc.* **2005**, *127*, 7140−7147.
(24) De Yoreo, J. J.; Gilbert, P. U. P. A.; Sommerdijk, N. A. J. M.; Penn, R. L.; Whitelam, S.; Joester, D.; Zhang, H.; Rimer, J. D.; Navrotsky, A.; Banfield, J. F.; Wallace, A. F.; Michel, F. M.; Meldrum, F. C.; Colfen, H.; Dove, P. M. Crystallization by Particle Attachment in Synthetic, Biogenic, and Geologic Environments. *Science* **2015**, *349*, 6760−6760.
(25) Zhang, H.; Huang, F.; Gilbert, B.; Banfield, J. F. Molecular Dynamics Simulations, Thermodynamic Analysis, and Experimental Study of Phase Stability of Zinc Sulfide Nanoparticles. *J. Phys. Chem. B* **2003**, *107*, 13051−13060.
(26) Banfield, J. F.; Welch, S. A.; Zhang, H.; Ebert, T. T.; Penn, R. L. Aggregation-Based Crystal Growth and Microstructure Development in Natural Iron Oxyhydroxide Biomineralization Products. *Science* **2000**, *289*, 751−754.
(27) Liao, H. G.; Cui, L.; Whitelam, S.; Zheng, H. Real-Time Imaging of Pt3Fe Nanorod Growth in Solution. *Science* **2012**, *336*, 1011−1014.
(28) Wang, F.; Richards, V. N.; Shields, S. P.; Buhro, W. E. Kinetics and Mechanisms of Aggregative Nanocrystal Growth. *Chem. Mater.* **2014**, *26*, 5−21.
(29) Lee, J.; Yang, J.; Kwon, S. G.; Hyeon, T. Nonclassical Nucleation and Growth of Inorganic Nanoparticles. *Nat. Rev. Mater.* **2016**, *1*, 1−16.
(30) Yuk, J. M.; Park, J.; Ercius, P.; Kim, K.; Hellebusch, D. J.; Crommie, M. F.; Lee, J. Y.; Zettl, A.; Alivisatos, A. P. High-Resolution EM of Colloidal Nanocrystal Growth Using Graphene Liquid Cells. *Science* **2012**, *336*, 61−64.
(31) Zheng, H.; Smith, R. K.; Jun, Y.; Kisielowski, C.; Dahmen, U.; Alivisatos, A. P. Observation of Single Colloidal Platinum Nanocrystal Growth Trajectories. *Science* **2009**, *324*, 1309−1312.
(32) Schliehe, C.; Juarez, B. H.; Pelletier, M.; Jander, S.; Greshnykh, D.; Nagel, M.; Meyer, A.; Foerster, S.; Kornowski, A.; Klinke, C.; Weller, H. Ultrathin PbS Sheets by Two-Dimensional Oriented Attachment. *Science* **2010**, *329*, 550−553.
(33) Chen, Y.; Chen, D.; Li, Z.; Peng, X. Symmetry-Breaking for Formation of Rectangular CdSe Two-Dimensional Nanocrystals in Zinc-Blende Structure. *J. Am. Chem. Soc.* **2017**, *139*, 10009−10019.
(34) Liu, Y. H.; Wang, F.; Wang, Y.; Gibbons, P. C.; Buhro, W. E. Lamellar Assembly of Cadmium Selenide Nanoclusters into Quantum Belts. *J. Am. Chem. Soc.* **2011**, *133*, 17005−17013.
(35) Tsai, M. H.; Chen, S. Y.; Shen, P. Imperfect Oriented Attachment: Accretion and Defect Generation of Nanosize Rutile Condensates. *Nano Lett.* **2004**, *4*, 1197−1201.
(36) Penn, R. L.; Banfield, J. F. Imperfect Oriented Attachment: Dislocation Generation in Defect-Free Nanocrystals. *Science* **1998**, *281*, 969−971.
(37) Burton, W. K.; Cabrera, N.; Frank, F. C. The Growth of Crystals and the Equilibrium Structure of Their Surfaces. *Philos. Trans. R. Soc., A* **1951**, *243*, 299−358.
(38) Jin, S.; Bierman, M. J.; Morin, S. A. A New Twist on Nanowire Formation: Screw-Dislocation-Driven Growth of Nanowires and Nanotubes. *J. Phys. Chem. Lett.* **2010**, *1*, 1472−1480.

DOI: 10.1021/acsnano.8b00638
ACS Nano XXXX, XXX, XXX−XXX

(39) Morin, S. A.; Forticaux, A.; Bierman, M. J.; Jin, S. Screw Dislocation-Driven Growth of Two-Dimensional Nanoplates. *Nano Lett.* **2011**, *11*, 4449−4455.
(40) Meng, F.; Morin, S. A.; Forticaux, A.; Jin, S. Screw Dislocation Driven Growth of Nanomaterials. *Acc. Chem. Res.* **2013**, *46*, 1616−1626.
(41) Queisser, H. J.; Haller, E. E. Defects in Semiconductors: Some Fatal, Some Vital. *Science* **1998**, *281*, 945−950.
(42) Sun, C.; Paulauskas, T.; Sen, F. G.; Lian, G.; Wang, J.; Buurma, C.; Chan, M. K. Y.; Klie, R. F.; Kim, M. J. Atomic and Electronic Structure of Lomer Dislocations at CdTe Bicrystal Interface. *Sci. Rep.* **2016**, *6*, 27009.
(43) Anderson, P. M.; Hirth, J. P.; Lothe, J. *Theory of Dislocations*, 3rd ed.; Cambridge University Press, 2017.
(44) Khanikar, P.; Kumar, A.; Subramaniam, A. Image Forces on Edge Dislocations: A Revisit of the Fundamental Concept with Special Regard to Nanocrystals. *Philos. Mag.* **2011**, *91*, 730−750.
(45) Kumar, A.; Subramaniam, A. Stable Edge Dislocations in Finite Crystals. *Philos. Mag.* **2012**, *92*, 2947−2956.
(46) Nabarro, F. R. N. Dislocations in a Simple Cubic Lattice. *Proc. Phys. Soc. London* **1947**, *59*, 256−272.
(47) Khanikar, P.; Subramaniam, A. Critical Size for Edge Dislocation Free Free-Standing Nanocrystals by Finite Element Method. *J. Nano Res.* **2010**, *10*, 93−103.
(48) Narayan, J. Critical Size for Defects in Nanostructured Materials. *J. Appl. Phys.* **2006**, *100*, 34309.
(49) Liao, X. Z.; Zhou, F.; Lavernia, E. J.; Srinivasan, S. G.; Baskes, M. I.; He, D. W.; Zhu, Y. T. Deformation Mechanism in Nanocrystalline Al: Partial Dislocation Slip. *Appl. Phys. Lett.* **2003**, *83*, 632−634.
(50) Whitham, K.; Yang, J.; Savitzky, B. H.; Kourkoutis, L. F.; Wise, F.; Hanrath, T. Charge Transport and Localization in Atomically Coherent Quantum Dot Solids. *Nat. Mater.* **2016**, *15*, 557−563.
(51) Van Huis, M. A.; Kunneman, L. T.; Overgaag, K.; Xu, Q.; Pandraud, G.; Zandbergen, H. W.; Vanmaekelbergh, D. Low-Temperature Nanocrystal Unification through Rotations and Relaxations Probed by *in Situ* Transmission Electron Microscopy. *Nano Lett.* **2008**, *8*, 3959−3963.
(52) Li, D.; Nielsen, M. H.; Lee, J. R. I.; Frandsen, C.; Banfield, J. F.; De Yoreo, J. J. Direction-Specific Interactions Control Crystal Growth by Oriented Attachment. *Science* **2012**, *336*, 1014−1018.
(53) Evers, W. H.; Goris, B.; Bals, S.; Casavola, M.; De Graaf, J.; van Roij, R.; Dijkstra, M.; Vanmaekelbergh, D. Low-Dimensional Semiconductor Superlattices Formed by Geometric Control over Nanocrystal Attachment. *Nano Lett.* **2013**, *13*, 2317−2323.
(54) Matthews, J. W.; Isebeck, K. Dislocations in Evaporated Lead Sulphide Films. *Philos. Mag.* **1963**, *8*, 469−485.
(55) Law, M.; Luther, J. M.; Song, Q.; Hughes, B. K.; Perkins, C. L.; Nozik, A. J. Structural, Optical, and Electrical Properties of PbSe Nanocrystal Solids Treated Thermally or with Simple Amines. *J. Am. Chem. Soc.* **2008**, *130*, 5974−5985.
(56) Blackburn, J. L.; Chappell, H.; Luther, J. M.; Nozik, A. J.; Johnson, J. C. Correlation between Photooxidation and the Appearance of Raman Scattering Bands in Lead Chalcogenide Quantum Dots. *J. Phys. Chem. Lett.* **2011**, *2*, 599−603.
(57) Kisielowski, C. Observing Atoms at Work by Controlling Beam-Sample Interactions. *Adv. Mater.* **2015**, *27*, 5838−5844.
(58) Van Dyck, D.; Lobato, I.; Chen, F. R.; Kisielowski, C. Do You Believe That Atoms Stay in Place When You Observe Them in HREM? *Micron* **2015**, *68*, 158−163.
(59) Kisielowski, C.; Wang, L. W.; Specht, P.; Calderon, H. A.; Barton, B.; Jiang, B.; Kang, J. H.; Cieslinski, R. Real-Time Sub-Ångstrom Imaging of Reversible and Irreversible Conformations in Rhodium Catalysts and Graphene. *Phys. Rev. B: Condens. Matter Mater. Phys.* **2013**, *88*, 1−12.
(60) Schober, T.; Balluffi, R. W. Quantitative Observation of Misfit Dislocation Arrays in Low and High Angle Twist Grain Boundaries. *Philos. Mag.* **1970**, *21*, 109−123.
(61) Siems, R.; Delavignette, P.; Amelinckx, S. The Buckling of a Thin Plate due to the Presence of an Edge Dislocation. *Phys. Status Solidi B* **1962**, *2*, 421−438.
(62) Kroupa, F. Die Abhangigkeit Der Banddurchbiegung Von Der Lage Der Stufenversetzung. *Czech. J. Phys.* **1959**, *9*, 488−494.
(63) Hofmann, F.; Abbey, B.; Liu, W.; Xu, R.; Usher, B. F.; Balaur, E.; Liu, Y. X-Ray Micro-Beam Characterization of Lattice Rotations and Distortions due to an Individual Dislocation. *Nat. Commun.* **2013**, *4*, 2774.
(64) Joo, J.; Son, J. S.; Kwon, S. G.; Yu, J. H.; Hyeon, T. Low-Temperature Solution-Phase Synthesis of Quantum Well Structured CdSe Nanoribbons. *J. Am. Chem. Soc.* **2006**, *128*, 5632−5633.
(65) Yu, J. H.; Liu, X.; Kweon, K. E.; Joo, J.; Park, J.; Ko, K. T.; Lee, D. W.; Shen, S.; Tivakornsasithorn, K.; Son, J. S.; Park, J. H.; Kim, Y. W.; Hwang, G. S.; Dobrowolska, M.; Furdyna, J. K.; Hyeon, T. Giant Zeeman Splitting in Nucleation-Controlled Doped CdSe:Mn2+quantum Nanoribbons. *Nat. Mater.* **2010**, *9*, 47−53.
(66) Schliehe, C.; Juarez, B. H.; Pelletier, M.; Jander, S.; Greshnykh, D.; Nagel, M.; Meyer, A.; Foerster, S.; Kornowski, A.; Klinke, C.; Weller, H. Ultrathin PbS Sheets by Two-Dimensional Oriented Attachment. *Science* **2010**, *329*, 550−553.
(67) Khan, A. H.; Pal, S.; Dalui, A.; Pradhan, J.; Sarma, D. D.; Acharya, S. Solution-Processed Free-Standing Ultrathin Two-Dimensional PbS Nanocrystals with Efficient and Highly Stable Dielectric Properties. *Chem. Mater.* **2017**, *29*, 1175−1182.
(68) Acharya, S.; Das, B.; Thupakula, U.; Ariga, K.; Sarma, D. D.; Israelachvili, J.; Golan, Y. A Bottom-up Approach toward Fabrication of Ultrathin PbS Sheets. *Nano Lett.* **2013**, *13*, 409−415.
(69) Treml, B. E.; Savitzky, B. H.; Tirmzi, A. M.; Dasilva, J. C.; Kourkoutis, L. F.; Hanrath, T. Successive Ionic Layer Absorption and Reaction for Postassembly Control over Inorganic Interdot Bonds in Long-Range Ordered Nanocrystal Films. *ACS Appl. Mater. Interfaces* **2017**, *9*, 13500−13507.
(70) Saka, H.; Imura, T. Direct Measurement of Mobility of Edge and Screw Dislocations in 3% Silicon-Iron by High Voltage Transmission Electron Microscopy. *J. Phys. Soc. Jpn.* **1972**, *32*, 702−716.
(71) Singh, R. N.; Coble, R. L. Dynamic Dislocation Behavior in " Pure " Magnesium Oxide Single Crystals *. *J. Appl. Phys.* **1974**, *45*, 981−989.
(72) Johnston, W. G.; Gilman, J. J. Dislocation Velocities, Dislocation Densities, and Plastic Flow in Lithium Fluoride Crystals. *J. Appl. Phys.* **1959**, *30*, 129−144.
(73) Zhu, X.; Liu, Z.; Shi, G.; Gu, J.; Wang, W.; Ma, W. Photovoltaic Devices Employing Ternary PbSxTe1-X Nanocrystals. *J. Mater. Sci. Technol.* **2017**, *33*, 418−423.
(74) Regan, W.; Alem, N.; Alemán, B.; Geng, B.; Girit, Ç.; Maserati, L.; Wang, F.; Crommie, M.; Zettl, A. A Direct Transfer of Layer-Area Graphene. *Appl. Phys. Lett.* **2010**, *96*, 11−13.
(75) Yuk, J. M.; Kim, K.; Aleman, B.; Regan, W.; Ryu, J. H.; Park, J.; Ercius, P.; Lee, H. M.; Alivisatos, A. P.; Crommie, M. F.; Lee, J. Y.; Zettl, A. Graphene Veils and Sandwiches. *Nano Lett.* **2011**, *11*, 3290−3294.

DOI: 10.1021/acsnano.8b00638
ACS Nano XXXX, XXX, XXX−XXX